MODELING OF PRESSURE DYNAMICS DURING SURGE AND ESD

Elisabetta Belardini
Senior Engineer
GE Oil & Gas
Florence, Italy

Dante Tommaso Rubino
Engineering Manager
GE Oil & Gas
Florence, Italy

Libero Tapinassi
Engineering Manager
GE Oil & Gas
Florence, Italy

Marco Pelella
Engineering Manager
GE Oil & Gas
Florence, Italy.

Elisabetta Belardini is Senior Engineer of Radial Turbo machinery Performance within the Advanced Technology Division of GE Oil & Gas Company, in Florence, Italy. She is responsible of performance predictability and risk assessment of centrifugal compressors, stall investigation and modeling of system dynamics. Elisabetta joined GE in 2005 as Test Engineer, then moved in present role. Elisabetta received a M.S. degree with honor in Mechanical Engineering in 1996 and a Ph.D. in Energetics in 2000 from University of Florence followed by a four year post-doctoral research in the unsteady CFD simulation of turbo machinery rows..

Dr. Tommaso Rubino is currently the Manager of the Radial Turbo machinery Aerodynamic Design and Performance within the Advanced Technology Division of GE Oil & Gas Company, in Florence, Italy. His responsibilities include the aerodynamic design and the performance predictability of the GE Oil & Gas turbo-compressors and turbo-expanders product lines. Dr. Rubino joined GE in 2006 as Design Engineer in Centrifugal Compressor NPI team, then rolling in the Aero team upon creation of the Advanced Technology Organization, where he has been responsible of the aerodynamic design of new stage families for Centrifugal Compressors. Mr. Rubino received a B.S. and M.S. degree in Mechanical Engineering in 2002 and a Ph.D. degree in Mechanical Engineering in 2006 from Politecnico of Bari, and he graduated with honors in the Diploma Course program at the von Karman Institute in 2002

Libero Tapinassi is currently the Manager of Turbomachinery Aerodynamics and Heat Transfer department of Advanced Technology Division of GE Oil & Gas Company, in Florence, Italy. His responsibilities include the aero-thermal design activities related to the development of GE Oil&Gas turbomachinery product line. Mr. Tapinassi joined GE in 2003 as

Design Engineer in Centrifugal Compressor NPI team, then he has worked as Manager of Centrifugal Compressor Aerodynamic team supporting stage development and performance improvement programs. Mr. Tapinassi received a B.S. degree (Environmental Engineering, 2001) from the University of Florence in 2001.

Marco Pelella is Engineering Manager for System Operability of Centrifugal Compressor & Turbo expander Applications with GE Oil & Gas in Florence, Italy. He also holds the title of Senior Engineer. His responsibilities include the definition of Process Control Philosophy and Dynamic Simulations. Mr. Pelella graduated in Mechanical Engineering at University of Naples, Italy in 1997. He joined GE in 1999 as Design Engineer of centrifugal compressors then moving to roles of increasing responsibility first as design office Team Leader of integrally geared and pipeline compressors, then as centrifugal compressors design office Engineering Manager in Le Creusot, France and axial and centrifugal compressors design office Engineering Manager for LNG and Down Stream applications in Florence, Italy. He has authored or coauthored of three technical papers, in the area of materials, fluid dynamic and rotor dynamics of process centrifugal compressors. He presently holds four patents.

ABSTRACT

Centrifugal compressors operability at low flow is normally limited by the onset of surge that occurs when operating near maximum achievable pressure rise. Surge is characterized by large amplitude and periodic pressure oscillations in which the compressor can also experience a series of flow reversal and recovery.

Surge may happen when compressors are subjected to rapid transients. Examples are represented by the emergency shutdown (ESD) or a power failure. To prevent this from occurring, compressor stations are equipped with single or dual recycle systems using valves, which are required to quickly open in presence of ESD.

For the proper sizing of recycles valves and whole system

layout in general the estimation of surge inception and frequency during transients are key parameters especially for high-pressure centrifugal compressors and usually require the characterization of compressor pressure ratio curve including the reverse flow region. Spool dynamics is important to simulate ESD transients so also the torque law for the compressor needs to be provided and extended in the negative flow region. Usually pressure ratio and torque law are not available from experiments. A quite simple approach based on considerations about velocity triangles is analyzed in this paper and compared with experimental data. The approach is firstly assessed in the analysis of simple systems (one model test and a full scale compressor), both modeled according to the classical plenum-pipe description suggested by Greitzer. Computed pressure and speed trends are compared with experimental data from the dynamic pressure probes during surge and ESD. Kulite probes were installed in addition to the standard instrumentation in the test loops of the model test as also of the full scale string test. The curve extension model based on velocity triangles proved good accuracy in the simulation of dynamic behavior of those systems. The same method was also applied for the analysis of a more complex compression train equipped with four machines and modelled with a commercial tool for dynamic simulation of fluid systems. The results obtained showed good agreement with pressure and speed trends coming from site acquisition devices.

INTRODUCTION

Compressor surge is usually modelled by the low order state-space model developed by Moore and Greitzer [2]. According to this model the whole compression system (including compressor, pipes of different diameters, bending, coolers…) is basically represented as a plenum filled with compressible fluid, in which flow is at rest, connected to the environment by one or more control valves and to the compressor by the pipe in which it is installed. The fluid is assumed uncompressible in the pipes where compressor and valves are installed and compressible inside the plenums. In spite of its extreme simplicity, this model showed good capabilities in predicting both the existence and nonlinear features of rotating stall and surge. Important applications have been documented (TNO [14] and MIT [1]).

With this approach it is not possible to account for many details of complicated systems as also propagation of pressure waves which may be important from an aero-acoustic point of view. Anyway for verification and design of simple systems the model proved to be accurate enough.

A critical point in the modeling of surge events is the extension of the characteristic curves with negative flow rates for which in general no test data are available and different assumptions can lead to different design choices. Two characteristic curves are necessary to the full simulation of ESD events. The first is represented by the pressure ratio-flow coefficient curve relating the pressure difference between upstream and downstream vessels to the mass flow of the compressor. For this characteristic a well agreed trend is the Gravdahl approach using a cubic interpolation between the leftmost operating point and the negative flow region. To capture speed trend also power absorbed during surge needs to be characterized: an

approach based on velocity triangles is described and indirectly validated against experimental data. The data used to validate curve left-extension are represented by a model test of a single stage compressor in which ESD and surge data are acquired for two different speed lines. Experimental curves are available only for the large flow coefficient stable range. Time accurate pressure fluctuations and speed trends recorded during surge are used to give a general assessment of the methodology used for extended operating range.

The method based on velocity triangles can be also applied to full scale centrifugal compressors for the proper sizing of the control valve: a design criteria based on speed deceleration is used to size bypass valve and verify safe operating range of the system.

SYSTEM MODELING & CURVE EXTENSION

System model and equations

The circuit is modelled following the classical approach proposed by Greitzer [1]for axial compressors (see Figure 1). The inlet volume V1 is assumed equal to the sum of the volumes of all the elements located between the outlet of the control valve and the inlet section of the compressor. The outlet volume V2 includes all the volumes between compressor discharge and inlet section of the control valve. Gas temperature and pressure are assumed uniform and fluid velocity equal to zero. Pressure rise across the compressor is modeled as an actuator disk and is described by the experimental performance curves extended up to the left stable region [6]. It is also characterized by the fluid passage length L_c, the inlet area A_c to account for the inertia of the fluid in the compressor duct. Similarly the throttle valve is characterized by the relation between pressure difference and volume flow (classical quadratic law). Valve inertia parameters L_t and inlet area A_t can be also defined but usually are negligible.
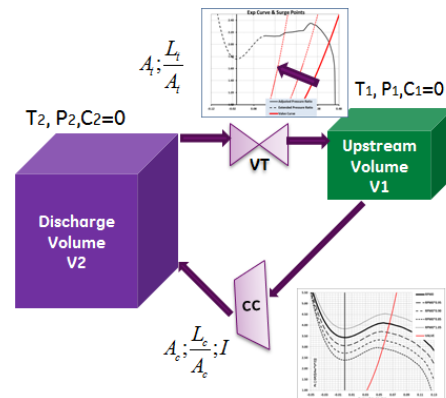

Figure 1 – Model of System Layout

Compressor is also characterized by the rotor angular momentum (I) in which the gas angular momentum in the compressor passages may be considered negligible. This last additional parameter is introduced to compute speed variations in the compressor train [2].

The system of equations describing surge modeling are well documented and explained in literature [2] so only the basic terminology will be briefly recalled here:

$$\begin{cases} \dfrac{\partial \varphi_c}{\partial \xi} = B\left[\psi_c(\varphi_c) - \psi\right] - \varphi_c LB\left(\overline{\Gamma}_{Driver} - \tau_{Gas}\varphi_c\right) & CC\ Mass\ Balance \\[2mm] \dfrac{\partial \psi}{\partial \xi} = \dfrac{F}{B}\left[\varphi_c - \varphi_t(\psi)\right] - 2LB\psi\left(\overline{\Gamma}_{Driver} - \tau_{Gas}\varphi_c\right) & Volume\ Pressure \\[2mm] \dfrac{\partial B}{\partial \xi} = LB^2\left(\overline{\Gamma}_{Driver} - \tau_{Gas}\varphi_c\right) & Rotor\ Equation \end{cases}$$

Equation 1

The model parameters B, F and L in Equation 1 will be separately addressed in the next paragraph. Ψ, Ψ_c and Ψ_t are the non-dimensional pressure differences between P_2 and P_1, the pressures in the upstream and downstream volumes, across compressor and the valve.

$$\psi = \frac{P_2 - P_1}{0.5\rho_{01}U_2^2} \qquad \psi_c = \frac{\Delta P_c}{0.5\rho_{01}U_2^2} \qquad \psi_t = \frac{\Delta P_t}{0.5\rho_{01}U_2^2}$$

All pressures are made non dimensional using the quantity $0.5\rho_{01}U_2^2$ in which U_2 is the impeller tip speed and ρ_{01} is the total density in the upstream volume at start time.

Flow coefficients φ_c and φ_t are the non-dimensional flow rates across compressor and valve respectively:

$$\varphi_c = \frac{M_c}{\rho_{01}U_2A_c} \qquad \varphi_t = \frac{M_t}{\rho_{01}U_2A_t}$$

The work coefficient τ_{Gas} is the non-dimensional work required by the compressor and includes both the energy transmitted to the gas and that absorbed by the rotor (mainly friction by ventilation). The total torque absorbed by compressor can be computed as $\tau_{Gas} \cdot \varphi_c$ while $\overline{\Gamma}_{Driver}$ is the non-dimensional torque provided by the driver:

$$\tau_{Gas} = \tau_c + \tau_{Friction} \qquad \overline{\Gamma}_{Driver} = \frac{\Gamma_{Driver}}{\rho_{01}U_2^2A_cR_2}$$

Time t is made non-dimensional time with the Helmholtz frequency ω_H :

$$\xi = t\omega_H \qquad \omega_H = c_2\sqrt{\frac{A_c}{V_2L_c}}$$

The regulation curve of V_T is required in order to compute the mass flow for each operating point:

$$\varphi_t = 0.25 \cdot u_r\sqrt{\overline{\rho}_2\psi_t}$$

Valve flow coefficient is assumed to be linear with the valve opening u_r, while it is related to both non dimensional density $\overline{\rho}_2$ and pressure difference ψ_t by the classical square relation.

A numerical sensitivity analysis showed that the exact evaluation of $\varphi_t = f(\psi_t)$ has limited effect on surge frequency and pressure oscillations even if may impact the pressure evolution during ESD.

This system of Equation 1 is integrated in time for the different operating points imposed by the valve openings u_r.

Applications are reported in which stall transient are accounted in the model of the compressor [7] and [8]. The mentioned experiences in the field of axial compressors show that characteristic curves are different depending on whether in presence or not of rotating stall. Stall cell blockage is a parameter computed on the base of experimental data of stalled flow and is used to evaluate the impact on the overall compressor performance. In present applications the magnitude of the rotating stall pressure fluctuations is seen to be small relative to the fluctuations due to surge. The rotating stall

disturbances thus appear, for this type of machines, to have little impact on the surge inception process.

In the surge and ESD simulations that will be reported in next sections both stall and time constants are neglected: the main focus is the verification of literature correlations for the curve extension and surge frequency prediction. Besides the trends of pressure fluctuations for those specific applications seems to confirm that the stall frequency has a poor impact on the steady state performance curves.

Model parameters

In Equation 1 three fundamental parameters can be identified:

$$B = \frac{U_2}{2c_2}\sqrt{\frac{V_2}{A_cL_c}} = bU_2 = b\omega R_2 \qquad Stability$$

$$L = \frac{2\rho_{01}A_cL_cR_2^2}{I} \qquad Inertia$$

$$F = 1 + \frac{Z_1T_1V_2}{Z_2T_2V_1} \qquad Suct.-Disch\ Coupling$$

The first equation describes the <u>stability parameter B</u>, which relates pressure variations in the volumes and flow rates in the valves. High values of this parameter are associated to big discharge volumes or high compressor tip speed and indicate low sensitivity of the outlet pressure to the mass flow variations and thus circuits where system inertia is high and surge frequency quite low (in the order of one or more seconds). The stability parameter B depends on the compressor duct length L_c and reference area A_c. Reference area is generally replaced by the hydraulic inductance (L_c/A_c) of the compressor which is computed as an integral along the flow path inside the machine $(L_c/A_c) = \int dl/A$. These parameters are used to model the fluid-dynamic inertia of the compressor and connecting ducts but their values are quite difficult to be computed due to the complex flow path inside a centrifugal compressor stage. More frequently the value of B is used as tuning parameter to obtain a good match between measured and simulated surge oscillations. In the applications reported in next chapters the theoretic values needed no correction to match the frequency of surge phenomena. The stability parameter is proportional to tip velocity U_2 and so changes in time according to the rotor speed and the balance between driver and resistant torque of the spool.

<u>The inertia parameter L</u> is the ratio between gas and rotor inertia (I): if rotor inertia is high lower speed variations are caused by the unbalance between the powers provided by the driver and absorbed by the rotor respectively. Actually the relation between the net output power from driver and the compressor power should be known: this includes coupling, friction, and transmission efficiencies, between the power turbine and the gas compressor.

<u>The coupling parameter F</u> accounts the interactions between discharge and suction side volumes to regulate pressure difference across the compressor. In presence of an inlet plenum with infinite volume the ratio $V_2/V_1 \rightarrow 0$ and $F \rightarrow 1$. With a finite inlet volume the value of F is always higher than unity so that pressure difference between inlet and outlet volumes changes faster with respect to the system with the plenum. During flow reversal while pressure in the discharge volume is reducing due to the emptying of outlet volume, the

suction pressure is evidently increasing with filling as a consequence of finite volume. The time required for a surge cycle is lower as the value of coupling parameter increases.

Compressor Extended Characteristics

In the system of equations two performance curves are required to characterize compressor behavior:

$$\begin{cases} \psi_c = \psi(\varphi_c) & head\ coeff \\ \tau_c = \tau(\varphi_c) & work\ coeff \end{cases}$$

The head coefficient ψ_c relates pressure difference between volumes to the flow coefficient φ_c, which in turn is associated to the work coefficient τ_c and the energy transferred to the fluid across the compressor. In order to model surge phenomenon, the complete steady characteristics of the compressor beyond the surge point and into the negative flow are required. Of course the two curves and their derivatives are easily predicted or measured in the direct flow stable region. For reverse flow stable conditions the availability of reliable experimental data is uncommon due to the inherently unsteady operations [2]. Various strategies are proposed for the numerical computation of extended head and work coefficients in steady state conditions. In reality during surge head and work at a given flow coefficient may differ [15] from the steady state characteristic. Unsteady left extended performance may be obtained by measurements; however, it requires the compressor to undergo controlled surge cycles for an extended period of time. A physically realistic and commonly used representation of left extended characteristic is the simple cubic law proposed by Moore & Greitzer [6]:

$$\psi_c = \psi_{c0} + H\left[1 + \frac{3}{2}\left(\frac{\varphi}{W} - 1\right) - \frac{1}{2}\left(\frac{\varphi}{W} - 1\right)^3\right]$$

$$\psi_{c0} = \left[1 + \frac{\pi^2(N/60)^2(D_2^2 - D_1^2)}{2C_{P12}T_2}\right]^{\left(\frac{\gamma}{\gamma-1}\right)}$$

Equation 2

$$W = 0.5 \cdot \varphi_c^* \qquad\qquad H = 0.5 \cdot \left(\psi_c^* - \psi_{c0}\right)$$

The equation parameters ψ_{C0} H and W are identified in Figure 2: ψ_{c0} is the compressor head at zero flow computed according to [6], W is half of the actual flow through the compressor at the surge point φ_c^* and H is half the difference between the head at surge and at zero flow $\psi_c^* - \psi_{c0}$.
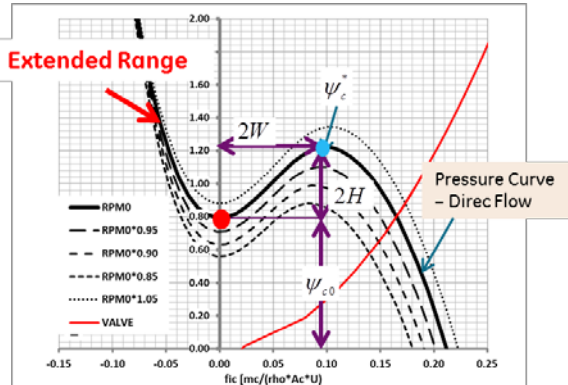
Figure 2 – Head Curve Extension

Full 3D Navier-Stokes time-accurate calculations for surge and rotating stall in 9-stage axial compressors have been reported

by [11]. The computational power required for these types of calculations is relevant and may not be possible to have it routinely available. An approximate estimation of absorbed energy during surge transients can be performed based on velocity triangles as suggested by [10] and [12] for turbine and axial compressors respectively. A method is proposed by [12] to reproduce the entropy generated by the large separations that are present within a blade passage during reverse-flow (negative axial velocity) conditions: the method assumes a flow separation at the trailing edge of the rotor with a blockage factor associated. Moreover, a jet-wake structure is produced at the rotor leading edge (direct flow terminology is retained) and supposing a perfect mixing of the two streams total pressure losses can be computed. In this model blade rows are approached as cascades of flat plates and flow is considered incompressible. This hypothesis is quite representative of the geometry for blades of axial compressors, in which both curvature and cross sectional area variations are limited. For centrifugal compressor blades this assumptions seem hardly applicable due to highly 3D contouring and stronger density variations between inlet and outlet section. From the blockage-mixing model proposed by [12] the blockage factor of the inlet area has been applied but the jet-wake structure in the outlet section has been considered fully mixed out.

1D model: velocity triangles approach

Velocity triangles and Euler equation are used in the computation of work coefficient based on the scheme reported in Figure 3a) for both direct and reverse flow:
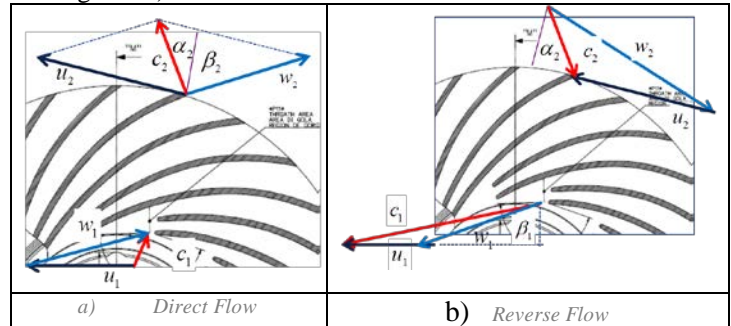
| a) | Direct Flow | b) | Reverse Flow |

#### Figure 3 – Velocity Triangles Direct & Reverse Flow

In direct flow at design point the velocity triangles at impeller outlet are represented in Figure 3a: the relative velocity w_2 is basically aligned to the blade trailing edge angle, forming the angle β_2 with the radial direction. With the contribution of the peripheral speed the absolute velocity from impeller is c_2. Static components downstream (mainly the return channel leading edge angle) are designed to match this outlet angle α_2 at the design flow coefficient. Work coefficient in direct flow can be computed as:

$$\tau_{Direct} = \frac{c_{t2}u_2 - c_{t1}u_1}{u_2^2} = 1 + \frac{\varphi}{4}\left(\frac{\rho_{01}}{\rho_2}\frac{D_2}{b_2}\tan\beta_2 - \frac{\rho_{01}}{\rho_1}\frac{D_2}{b_1}\tan\alpha_1\right)$$

Equation 3

During flow reversal it is assumed that the flow angle α_2 from return channel is approximately the same of the direct flow so that direction of c_2 is the same but opposite in sign (Figure 3b). Considering the same peripheral speed u_2 the resulting relative

velocity in reverse flow is w_2, higher in module with respect to direct flow and with a very large incidence angle with the rotor trailing edge (around 130°). Since the trailing-edge is relatively sharp, the flow is expected to generate a large separation zone within the vane passage before aligning to the blade surface (Figure 4a).

| a) Blockage Factor | b) Velocity Triangles inside vane |
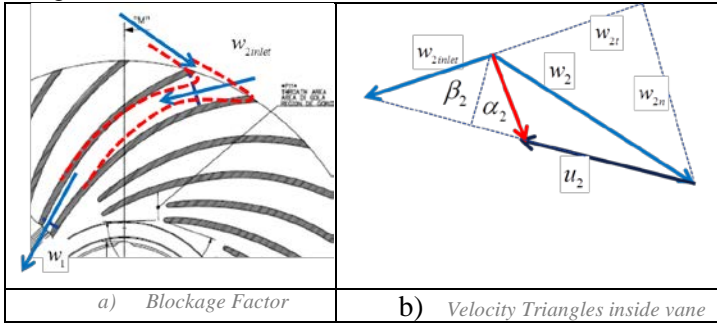
Figure 4 – Velocity Triangles: Incidence and Blockage

The effective area is only part of the geometric passage area and based on CFD computations a value equal to 60% has been assumed as blockage factor for all flow rates. The alignment of the velocity vector w_2 to the blade surface w_{2inlet} is assumed at constant total temperature and static pressure: great part of the kinetic energy of the flow outside the blade passage is dissipated causing an increase of static temperature and a strong decrease of total pressure with a remarkable entropy production.

As far as concerns the outlet section the flow is assumed quite uniform without a jet-wake structure considering the accelerating nature of the flow together with the length of the blade. A halved blockage factor equal to 0.3 at impeller leading edge is anyway retained to account the strong presence of secondary flows inside the vane passage. The relative velocity w_1 at impeller leading edge is aligned to the blade inlet angle β_1 so that the absolute velocity c_1 can be computed. The work coefficient in reverse flow $\tau_{Reverse}$ has the following expression:

$$\tau_{Reverse} = \frac{c_{t1}u_1 - c_{t2}u_2}{u_2^2} = \left(\frac{D_1}{D_2}\right)^2 + \frac{\varphi_1}{4}\left(-\frac{\rho_{02}}{\rho_1}\frac{D_2}{b_1}\tan\beta_1 + \frac{\rho_{02}}{\rho_2}\frac{D_2}{b_2}\tan\alpha_2\right)$$

Equation 4

In Figure 5a) and Figure 5b) the work and pressure coefficients in the extended operating range are shown for the 3D impeller of test case A that will be analyzed later.

| a) Work Coefficient | b) Pressure Ratio |
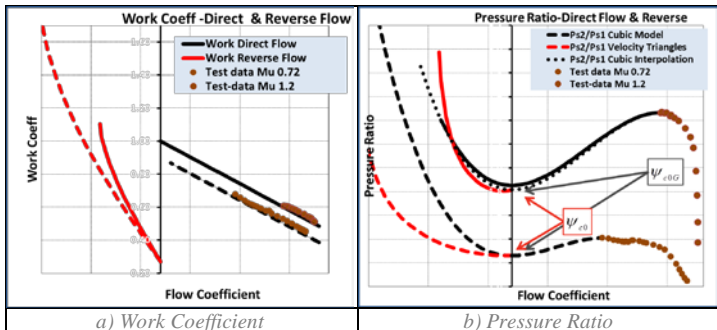
Figure 5 – Reverse Flow Performance Curves

Design flow coefficient and Mach number are equal to 0.1273 and 1.2 respectively. Two curves are reported for the design

Mach number equal to 1.2 (continuous lines) and the off design at 0.72 (dashed lines). The brown dots are the measured points in direct stable flow for both speed-lines. The extension of work coefficient at low flow in unstable region is done linearly up to the point at zero flow where work coefficient is close to one. The work coefficient in reverse flow is computed according to Equation 4: at zero flow the value is equal to $(D_1/D_2)^2$ which for the specific application is around 0.27 so that a discontinuity across zero is present. The work coefficient increases rapidly for negative flows up to values higher than 1 for approximately half the of one the direct design flow coefficient. The slope of the work coefficient curve is higher in reverse with respect to the direct flow: in Equation 4 β_1 is negative and α_2 positive and both contributions are in the same direction. In Equation 3 for direct flow β_2 is negative and very close to β_1 while inlet flow angle α_1 is positive but generally very close to zero. At design speed chocking of the inlet section of impeller causes the abrupt raise of the work coefficient. In the off design curve the slope of the curve is lower due to a lower value of the compressibility term in Equation 4 and chocking happens with higher reverse flow coefficients.

In Figure 5b the computed pressure ratio is reported in the extended operating range for the same test case. The red curves are computed based on 1D model: continuous lines at the design Mach number and the dashed one for the off design. The black curves are computed according to the cubic extrapolation rule. For the design curve both the cubic interpolation and the 1D model are quite close even if the computed pressure ratio at zero flow ψ_{c0} using 1D method is around 4-5% lower than ψ_{c0G} computed according to Equation 2. A cubic interpolation trough ψ_{c0} (dotted line) is very close to the velocity triangle approach. For the off-design speed, computed pressure ratio at zero flow ψ_{c0} is aligned with ψ_{c0G} but the trend with flow coefficient indicates a higher flow coefficient for the same pressure ratio with respect to the cubic interpolation law. During reverse flow, a certain pressure difference between inlet and outlet volumes will cause higher reverse flow according to 1D method with a corresponding higher work coefficient or equivalently absorbed power. Computed power absorbed during a surge cycle is greater and tendency to speed increase during surge reduced. This aspect will be better analyzed in the chapter dedicated to model validation.

From a thermodynamic standpoint (Figure 6a) the gas inside the compressor undergoes a pressure decrease from the inlet 1 to the outlet 2 since flow is driven by the external pressure difference between the two volumes. The total temperature of the gas increases since the rotation direction remains unchanged and the motor is transmitting power. Velocity inside the impeller increases towards section 1 due to the reduction of cross sectional area with the diameter. Both static pressure and kinetic energy contribute to the final total pressure at the outlet section which can be in principle higher or lower than the inlet value. In present applications a very high entropy production is computed by the model of incidence losses at the impeller leading edge thus the value of total pressure is lower at the outlet with respect to the inlet. In the T-S diagram, the gas transformation is represented by the red arrow. In Figure 6b the same transformation is reported for a negative mass flow close

to the design one in direct operation. ==Increasing the amount of gas the work transmitted to the gas increases==
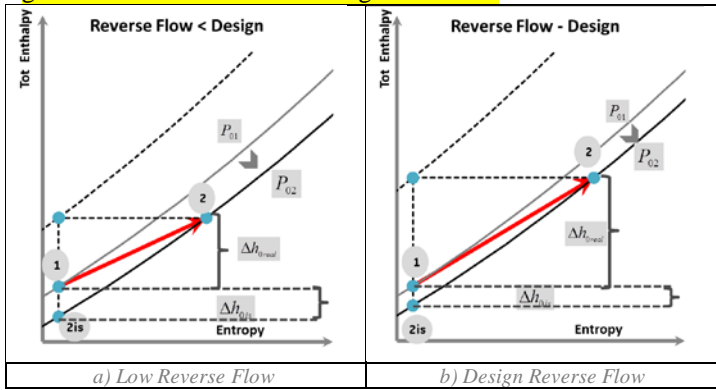

Figure 6 – Thermodynamics transformation in reverse flow

According to the standard definition of efficiency the outlet reference condition would be point 2is, corresponding to an isentropic expansion between the same total pressures. The enthalpy corresponding to the adiabatic reversible process is H_{02is}, lower with respect to is H_{01}. As a consequence the classical definition of the isentropic efficiency $\eta_{iso} = \Delta H_{0iso}/\Delta H_{0real}$ leads to negative values; in many conditions it can even exceed one in absolute value, especially with small reverse flows when the pressure difference is quite high but power absorption is still low (see Figure 6a). Referring to polytropic efficiency $\eta_{pol} = \Delta H_{0pol}/\Delta H_{0real}$, which is more frequent in the evaluation of centrifugal compressor performance, same considerations about the negative value and range over unity can be extended even if visualization in the T-S diagram is not as simple as for the isentropic efficiency. Moreover, the computation of polytrophic efficiency becomes implicit. An example of computed efficiency curves is reported in Figure 7 at different speeds, for the model test analyzed in next sections.
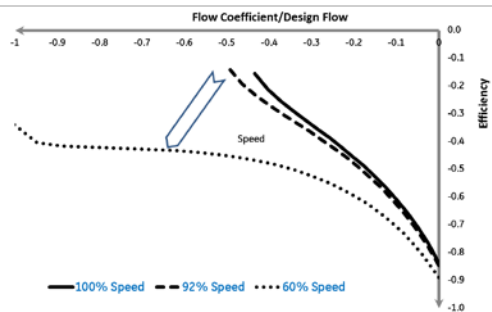

Figure 7 – Efficiency Curves in Reverse flow

At design speed in reverse flow efficiency can reach values around -0.9 close to zero flow; in this case the pressure difference applied between the two volumes is equal to the pressure difference to overcome centrifugal forces, total pressure variation is almost equal to the static pressure difference due to small variations of kinetic energy and the energy transmitted to the gas very close to the work by centrifugal forces. With increasing mass flow total pressure decrease across the impeller reduces due to the higher kinetic contribution of the outlet section: isentropic work decreases while the real one increase. The value of efficiency decreases accordingly up to values around -0.2. Of course these operating conditions of the compressor are very far from the design and

also the definition of efficiency is rarely acceptable: it has been mantained only for consistency with the positive flow branch of the characteristic curve.

VALIDATION ON MODEL TEST LOOP

In this section experimental data collected on a model test loop are used to verify the capability of the model described in previous section. Direct measurement of the stable performance map in the negative flow region has been successfully performed but requires in general quite big efforts in the design of the experimental layout which cannot be performed routinely. For this reason attention has been focused on validation of the negative flow stable operating curve using as much as possible surge and ESD data.

The test circuit is a standard closed loop test bench as showed in Figure 8a. The tested machine (Figure 8b) is a single stage compressor equipped with a 3D open impeller, a vaned diffuser and a discharge scroll. Test gas is pure CO_2, inlet temperature is around 293K while inlet pressure is in the range 1.2-2.3 bars.
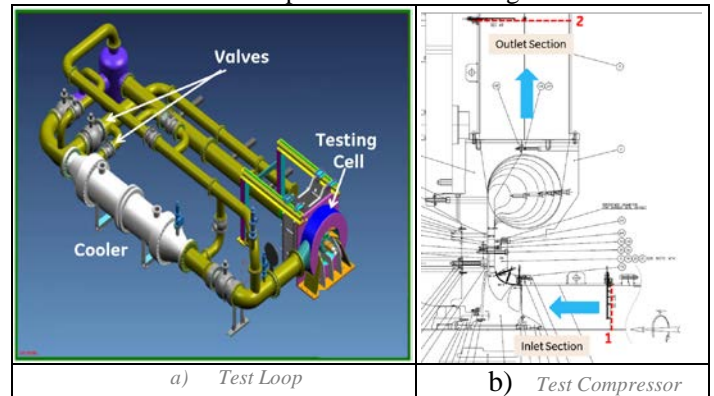

Figure 8 – Test layout and tested stage

In the test campaign the pressure trends have been recorded during ESD and SURGE at different peripheral Mach numbers. Exact test conditions of the cases analyzed are reported in Table 1.

Performance curves in the stable direct flow are measured by pressure and temperature Kiel probes: four rakes with four Kiel pressure and temperature probes are located in both inlet and outlet section, tangentially spaced of 90° as indicated in Figure 8b.

Table 1 – Test Conditions

	Surge @ Mu 1.2	Surge @ Mu 0.72	ESD @ Mu 1.10	4 Stage HP-CC
MW [kg/mol]	44.00	44.00	44.00	28.00
Gas	CO2	CO2	CO2	N2
Rgas [J/kg/k]	188.95	188.95	188.95	296.93
Kgas	1.29	1.29	1.29	1.39
Isoentropic Exponent	4.45	4.45	4.45	3.56
Mach	1.20	0.72	1.10	0.49
Cpgas [J/kg/k]	848.91	851.48	840.52	1058.28
P1[atm]	1.12	1.57	2.37	107.00
T1 [K]	298.22	292.21	294.80	296.82
Z1	0.994	0.991	0.994	1.013
T2 [K]	385.40	309.15	361.40	386.09
Z2	0.994	0.991	0.994	1.093
rho1 [kg/m3]	1.88	2.87	2.32	112.77
RPM [rev/min]	15762	9356	14609	
U2 [m/s]	321.87	191.05	298.32	172.00
B0	2.49	1.54	2.22	3.31
Wh	13.75	13.30	14.35	15.44
L0	0.0534	0.00967	0.0190	0.0097

Dynamic pressure signals are acquired during transients by two Kulite XTL-AC-190 pressure sensors located at both the inlet and outlet section of the compressor. At stage outlet, due to

geometry constraints, Kulite sensors are actually located inside the blue plenum shown in Figure 8e: the amplitude of pressure fluctuations may be smoothed with respect to the outlet section of the stage. At both impeller and vaned diffuser outlet PCB sensors are applied in order to detect additional pulsations connected to rotating stall. Three events will be analyzed in this context to validate dynamic model: two surge events at almost constant speed started at Mach number 1.2 and 0.72 and one ESD. Speed transients during surge are important for an indirect verification of key features of curve extension procedure while the deceleration rate during ESD can be used for basic assessment of rotor inertia modeling. The test data for the anti-surge design verification case for a four stage compressor, reported in following section, are also listed in Table 1.
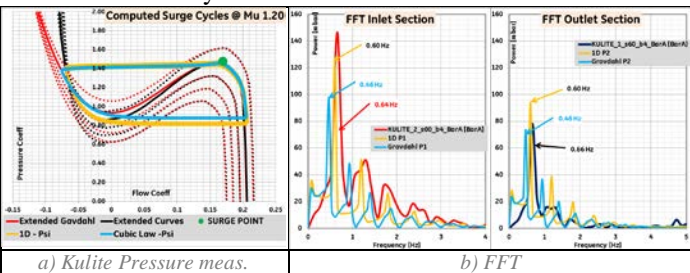
Surge @ Mu=1.20

In Figure 9a pressure fluctuation trends for inlet and outlet pressure are shown during surge event from Kulite measurements: blue curve is referred to the outlet section and red one to the inlet one. In Figure 9b pressure fluctuations detected by PCB sensors located at outlet of impeller and diffuser outlet are shown. Both signals indicate high frequency content in the pulsations when approaching the left limit of the curve corresponding to the point of maximum pressure.

a) Kulite Pressure meas. | *b) PCB fluctuations*
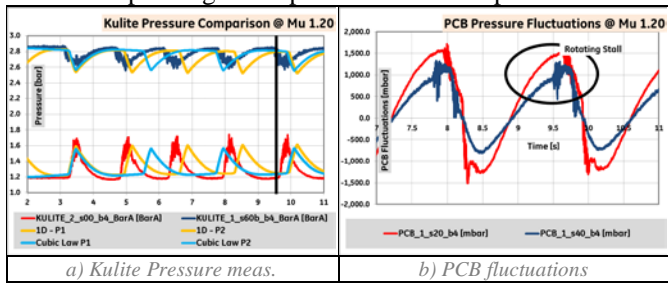
Figure 9 - Comparison @ Surge Mu 1.20

These pulsations are likely associated to a rotating stall inception triggering surge phenomena in each cycle and are in fact less evident in the Kulite signals. Their amplitude seems smaller compared to the amplitude of pressure fluctuations during surge cycle. This is consistent with the high values of inertia B parameter for this test case (2.49) and justifies the fact that in the system modeling equations no stall correction is applied to static performance during surge dynamics. High frequency pressure fluctuations can be detected also from Kulite sensors during flow reversal and are probably related to reflection of the rapid pressure fluctuation associated to flow inversion [3]. Flow reversal takes place in around 0.05s and can be considered as a sort of shock wave while cooler may act as a reflection boundary

*a) Kulite Pressure meas.* | *b) FFT*

Figure 10 - Comparison @ Surge Mu 1.20

In Figure 9a) and Figure 10 computed pressure trends are shown and compared with the measured signal: orange lines are obtained using 1D model approach to extend performance curves while the blue ones are based upon the cubic interpolation (see Figure 2). In Figure 10a) surge loops are described in the pressure ratio versus flow coefficient performance maps. The two considered extension methods lead to very similar paths for this test case: the point of minimum pressure ratio is slightly lower with the 1D method and the pressure curve a bit steeper.

In Figure 9a) pressure fluctuations associated to surge are compared with experiments. The computed amplitude of surge pressure fluctuations is related mainly to the difference between the point of minimum and maximum pressure ratio corresponding to the last stable points on the left and the pressure ratio at zero flow. In this regard the amplitude of the experimental pressure fluctuations can be used to verify the minimum pressure ratio point. For this test case the computed amplitudes of pressure fluctuations are quite close: 120 and 100 mbar respectively for the two methods in the inlet section. In Figure 10b) the measured frequency spectrum is shown: main frequency content of the experimental signal during surge is represented by 0.64 Hz and its harmonics. Time required to fulfill a surge cycle for a fixed system is mainly related to the shape of the stable portions of the performance curve with negative slope while time spent in the unstable branches is approximately one order of magnitude lower. In Figure 10a) surge loops computed with 1D approach is characterized by the same positive stable region but a longer negative branch. This difference causes a lower predicted surge frequency of 0.60Hz in comparison with that computed with standard extension 0.46Hz. For this test case close to the design Mach number both models show a good capability in predicting surge basic features.

Surge @ Mu=0.72

In Figure 11 pressure trends during surge are shown from both Kulite and PCB sensors for an off-design speed-line at Mu=0.72 at around 9400 RPM (B=1.54). Compared with the previous case the amplitude of pressure fluctuations due to surge is smaller in both inlet and outlet sections since scaling approximately with the speed square and linearly with pressure. From PCB signals reported in Figure 11b) high frequency oscillations at impeller outlet are present in both forward and backward stable range: these pressure fluctuations are much smoothed at diffuser outlet so they are realistically due to a rotating stall henomena.

a) Kulite Pressure meas. | *b) PCB fluctuations*
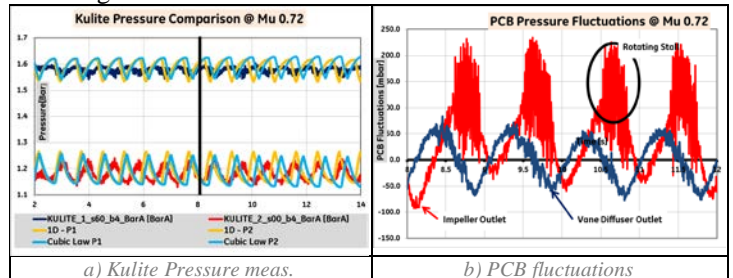
Figure 11 - Comparison @ Surge Mu 0.72

In Figure 11a) experimental signals are compared with those computed with both the 1D and cubic methods: in this case the extended curves as shown in Figure 12 are quite different as
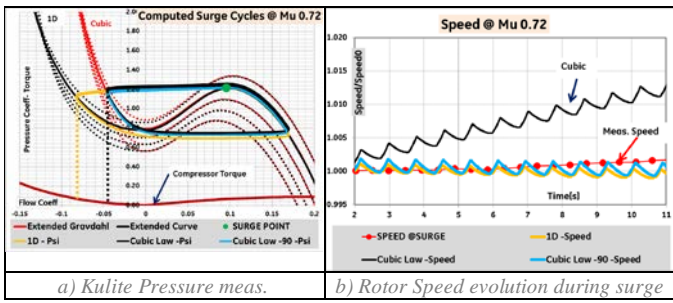
already commented in Figure 5.

| a) Kulite Pressure meas. | b) Rotor Speed evolution during surge |

Figure 12 - Comparison @ Surge Mu 0.72

With the 1D method the maximum negative mass at flow reversal is higher due to the smoother slope of the pressure ratio characteristic. As a consequence during the reverse flow operation of the compressor a higher torque is applied to rotor by the gas (out of scale for graphical reasons) when operating at maximum negative flow rate. The major effect of absorbed torque is reflected by the trend of the rotor speed during surge. Figure 12b) reports the instantaneous speed divided by the value at surge inception versus time. The experimental speed is represented by the dotted red line and is almost constant during all surge operations except for a speed increase of around 0.1% which can be noticed after 11s. The tendency towards acceleration of the rotor is quite common in surging systems and is associated to the lower average gas torque during a surge cycle with respect to that of surge point in stable operating conditions. If driver torque is not promptly reduced rotor tends to undergo a certain acceleration rate. In this system the acceleration is very small considering also the low value of inertia L characterizing the system. The orange line in Figure 12b is the trend of rotor speed computed using the 1D method which is in good agreement with the trend of average speed. Sampling of the speed signal is 0.47s while the surge cycle is 0.9s so the exact shape of speed trend during a surge cycle cannot be accurately tracked by the experiments. The average speed with cubic extension law (black line) tends to increase with a rate of 1% in 10s: the maximum reverse flow coefficient is 0.045 with an average torque 0.0587 during a surge cycle. If accordingly the driver torque is reduced of 10% the blue line is obtained and computed trend falls closer to the experimental speed trend. In the 1D extension the average torque in the surge cycle is 0.0660 which is much closer to the value of 0.0655 corresponding to the stable operating condition. In Figure 11 a slight trend of system pressures, decreasing and increasing for the upstream and downstream respectively can be noticed. These trends are related to the computed increase of speed for the cubic interpolation. In off design conditions the comparison of the computed speed trend with the experiments could be used as an indirect verification of the power absorption law in negative flow. The work coefficient trend coupled with the pressure ratio with velocity triangles showed a good accuracy in the off design Mach number with both pressure fluctuation and speed trend with time. The cubic law gives a sufficient accuracy in terms of pressure fluctuations even if the speed is around 1% after 9s. As far as concerns the amplitude and frequency of pressure fluctuations the approach showed some inaccuracy.

In Figure 13 the comparison of computed and measured pressure fluctuations are reported: in this case both surge frequency and power are overestimated in the computations especially in the outlet sections. The reason may be related to the assumption that the blockage factor used to compute performance in reverse flow is not taking into account off design speed-lines. With lower Mach also tangential velocity decreases leading to a lower incidence at impeller outlet and blockage should account for this (see Figure 4). Actually no correction is available to account this effect. Another critical point is the modeling of stall impact on the steady state characteristics: in this case PCB signals indicate an important fraction of the surge cycle with stalled flow. This may require the introduction of a stalled characteristic with lower pressure ratio [8]. Other possible issue is proper estimation of the global inertia of the train during dynamic conditions: speed is regulated by a fluid drive whose characteristics are not perfectly monitored during transients.
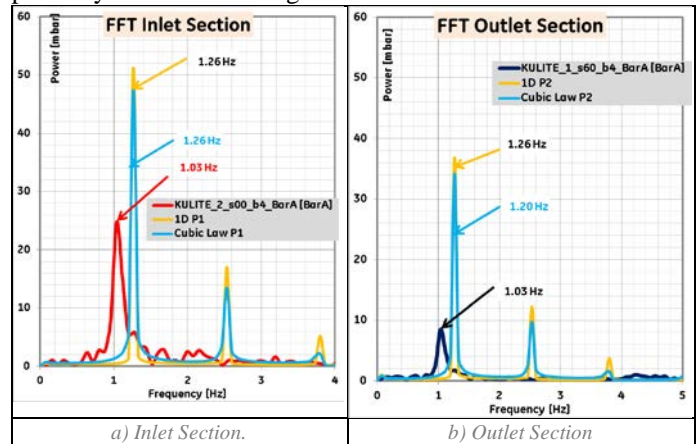

| a) Inlet Section. | b) Outlet Section |

Figure 13 - FFT @ Surge Mu 0.72

ESD @ Mu=1.10

The ESD event occurred due to high temperature at bearings at Mu=1.10, inlet pressure of 2.3bars and rotating speed around 14600 RPM. With these conditions stability B and inertia L parameters are 2.22 and 0.0191 respectively. The operating point at trip was quite close to surge limit of the curve (see Figure 15) so during rotor deceleration surge line is reached and reverse flow is experienced by the compressor for about 0.2s. During the following direct flow phase of the surge cycle the rapid deceleration of the rotor forces the operating point on the stable positive branch of the performance curve. In Figure 14a) and Figure 14b) speed during ESD and pressure traces from Kulite sensors are shown versus time. Speed has been made non dimensional with the initial value. ESD events are important for the assessment of the model capability in reproducing speed trends together with pressure variations in the system. Rotor deceleration is almost completely driven by inertia parameter of the system (Equation 1) and the net torque $\overline{\Gamma}_{Driver} - \tau_{Gas}\varphi_c$. In particular, since during trip the driver torque is zero, the contribution of friction torque may become important. In present application the classical formula proposed by Daily and Nece (1960a and 1960b) is used.

In Figure 14a) the experimental trend of the speed seems well reproduced up to a ratio of 0.20 between actual and initial speed. In particular time required to reduce speed up to 60% which is around 5s is properly captured: this parameter is used as a criteria to assess safety of a given circuit layout or to select

regulation valve for new applications. The trend has been obtained assuming that the inertia of the fluid drive decreases with a quadratic law. As far as concerns the pressure trends it seems that the trend is quite well captured in the first 4s after which equalization between two volumes seems to be too fast: this may be associated to the linear law between pressure and flow assumed for the unknown valve-travel relation which may be accurate when pressure difference is high but may overestimate the mass flow with smaller pressure differences.
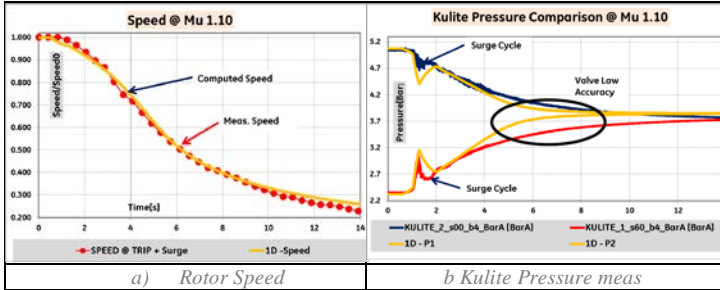
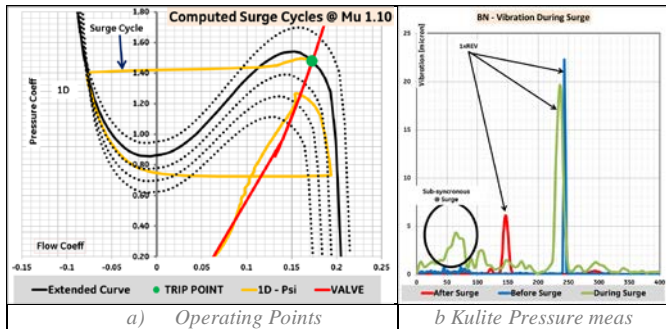*Figure 14 – Surge Cycle @ ESD*

Figure 15 – Surge Cycle @ ESD

In Figure 15 vibration during surge are shown: the blue and red curves are referred to instants before and after surge respectively and the frequency corresponding to the rotational speed is the most important content. The green curve is the frequency spectrum during the reverse flow period and a frequency around 25% of rotational speed can be detected. This frequency is also present in the PCB signals and to the authors' opinion can be connected to a rotating stall in stable reverse flow originated by the high incidence angle between velocity and blade angle. The rotating forces associated to the stalled cells are responsible for the vibrations detected by at the bearings by the BN sensors. The amplitude of these sub synchronous vibrations is much lower than those associated to the rotor speed close to the nominal conditions so that the reverse stable flow may appear less severe than a continuous looping system.

ANTISURGE DESIGN

The curve extension method of previous chapters can be used coupled with the 1D system of Equation 1 for transient simulations of simple systems such as a model test loop or ASME TYPE II test layout. For more complex systems the assumptions behind the Greitzer model of single volumes may be too restrictive and more advanced tools for dynamic modeling of fluid systems are used to properly reproduce circuit layout or acoustic behavior [3]. In both cases the extended curves in the reverse flow direct rotation are

important for the proper sizing of the bypass valve of the circuit in order to protect centrifugal compressor against surge during ESD. In this section an example of design practice for surge protection system and associated verification criteria are presented together with the comparison of the two different extension methods analyzed.

Design Criteria for Anti Surge System

The anti-surge valve is the standard tool to control and protect centrifugal compressors during normal operation (see Ref. 1). The design of anti-surge valve is a compromise between its potential to avoid surge which would require large valves, the controllability at partial recycle and the power of actuator which are less critical with smaller valves. In practical applications a guess value of the valve coefficient C_V is selected considering the head provided at design flow (Point A in Figure 16) and the volumetric flow corresponding to the intersection of the design head with the maximum speed performance curve (Point B).

$$C_V = \frac{Q_B}{K} \sqrt{\frac{\rho_{Des} T_{Des}}{\Delta P_{Des} \cdot P_{2Des}}}$$

Equation 5

In Equation 5 K is a coefficient depending on the system units. Actual valve size needs to be between 90% and 110% of the computed valve coefficient.
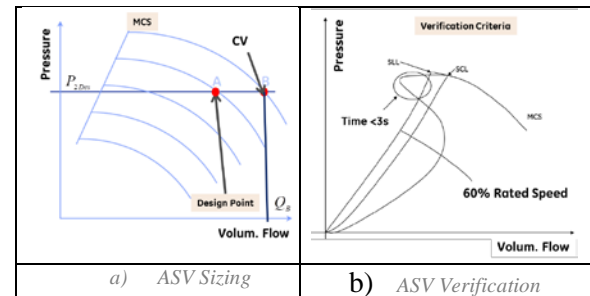

Figure 16 – ASV design and verification

ASV Verification

The suitability of selected anti-surge valve is verified simulating numerically an ESD event from the SLL and MCS. These situations represent the most severe scenario for surge protection systems since the compressor is operating with the minimum margin to surge and the maximum potential amplitude of the surge pressure fluctuations which scale with speed square. When the engine shutdown occurs compressor decelerates with a rate depending from the balance of the fluid forces and the inertia of the rotor system: deceleration is in the order of 50% drop of compressor speed within 3 seconds after the shutdown (see Figure 15). In this time, considering approximately a quadratic law between head and speed, the head reduction is about 75%. To avoid surge during this transient the ASV should reduce the pressure difference across the compressor with the same rate of the head reduction with speed. If the system volumes are relatively large the valve is not sufficient to avoid surge and additional devices such as recycle loops (cold or hot), check valves or different sizing of volumes may be considered to guarantee the criteria. In many of these cases the system layout is impacted in terms of cost and complexity.

The verification criteria is based on the widespread field experience that few surge cycles at constant speed can be undertaken by both compressor and system equipment without significant damages (critical cycles). Critical number of cycles depends on the size, operating conditions of the system and absorbed power. Based on this understanding an equivalent criterion based on time, more closely linked to valve opening features, can be derived as a verification criteria. Assuming that the surge cycle extent is in the order of 1 Hz, a centrifugal compressor is allowed operating on the left of the SLL (Surge Limit Line) and speeds above 60% of the rated for a number of seconds, critical time, and equal to the critical number of cycles. The rule on time is conservative in terms of potential damaging power with respect to the criterion based on surge cycles at constant speed. In fact during ESD the speed continuously decreases as well as the differential pressure across the compressor leading to a decrease of the energy associated to each surge oscillations. Besides not always seconds can be directly associated with cycles. With the large discharge volumes of typical systems the trajectory of the operating point evolves mostly in the second quadrant with stable reverse flow, in many cases without even displaying cycles. Coast down beyond SLL and below 60% of rated is accepted provided that no risk of reverse rotation is present.

The criterion based on critical time is a first verification step: if it is respected no further verification and additional protection device (i.e. HGB/CGB loop or ASV re-sizing or addition of suction/discharge check valves) are required. Otherwise additional verifications are done based on a qualitative parameter called Surge Sensitivity Number (SSN). This parameter estimates the impact of a surge event on compressor performance assuming high vibrations level as main failure mode. As a consequence of vibration rubbing of the seals and increase of clearances are detected and the impact on the guaranteed compressor performances is estimate. In case the SSN is lower than a certain threshold, the critical time can be doubled.

As a standard practice the numerical verification during ESD is done at two operating points: the one closest to the SCL and the one at highest operating speed. The first point is the most critical in terms of number of surge cycles while the point at MCS is that requiring larger time to reach 60% of design speed.

Application of ASV criteria

The design and verification rules for the ASV described in previous chapters have been applied to a high pressure compressor equipped with four impellers with an average external diameter of 275mm. The site working conditions and system model parameters are reported in Table 1 and the computed critical time for this application is 3s. The circuit is quite simple so 1D system of Equation 1 has been used for transient simulations coupled with both the 1D and cubic extension methods. Results in the pressure-flow coefficient plane are reported in Figure 17. The performance curves for the compressor at different speed-lines are represented by the black curves: continuous lines for nominal rpm and dotted ones for off design conditions. Anti-surge valve has been selected according to the design criteria of Equation 5 and the characteristic curve with full opening is represented by the red curve. Verification of ASV is done starting from the operating

point closest to the SCL at design speed, indicated by the green dot, at which an instantaneous trip of the driver happens. The blue curve represents the baseline path followed by the operating point in the pressure versus flow coefficient plane considering ASV closed during whole trip event. Compressor experiences a sudden flow inversion followed by a quite long route of stable operation in second quadrant. This is consistent with both to the high volumes involved in the system and the small size of the flow path inside the compressor, which lead to a stability parameter above 3. The green line in Figure 17 is the track of the operating point in case of full opening of ASV at the maximum speed endorsed by actuation system. In this case the pressure coefficient during the event is lower as a consequence of the faster emptying of discharge volume. The brown line is simulating the same event of the green one but is obtained using the cubic extension method for pressure ratio instead of the 1D model.
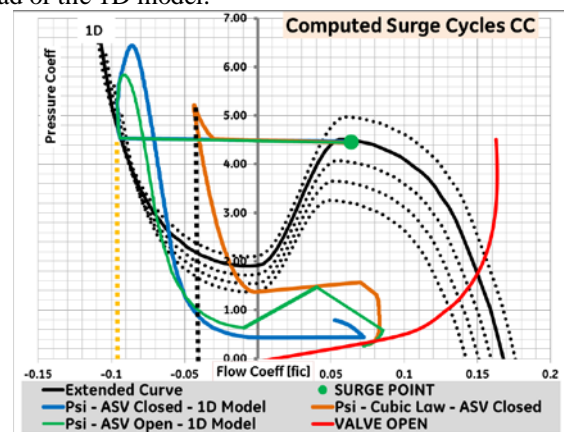

Figure 17 – Loop Cycle of Compressor

During operation in the second quadrant speed is progressively decreasing with time. The trends are reported in Figure 18 together with the traces of the flow coefficient. With both the closed and opened valve (dark blue and green lines respectively) the speed reduces to 60% after 2.97 seconds. Deceleration rate is mostly related to the inertia parameter L and the gas torque $\overline{\Gamma}_{Gas} = \tau_{Gas}\varphi_c$, according to system of Equation 1, but is practically unaffected by the opening of the valve. This time spent on the left of the SLL satisfies the verification criteria of 3s.
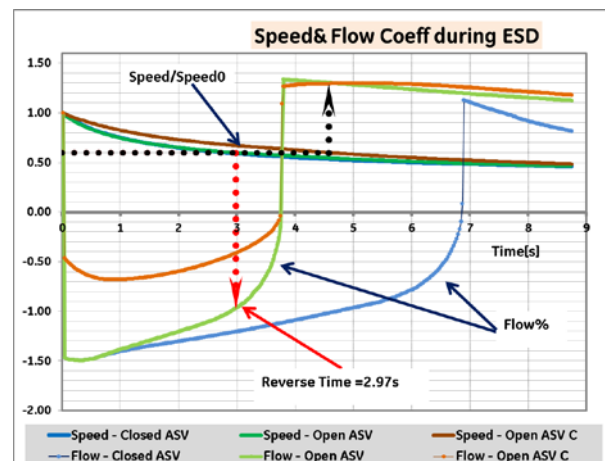

Figure 18 – Speed and flow trends during ESD

Total reverse time is different with closed and opened ASV: 7s

with closed valve (light blue line) reduces to around 3.75s with full opening of the ASV (light green line). The fast opening of the ASV increases the velocity at which pressure in the discharge volume reduces with respect to baseline case. In this case the limit point of negative stable region, corresponding to the minimum pressure at zero flow for a given speed-lines is reached faster. After the first reverse flow cycle, positive flow is restored without further surge cycles, with both shut down sequence with ASV opening or not.

Using the cubic extension method the brown lines of Figure 17 and Figure 18 are obtained. From Figure 17 the main difference is represented by the lower negative flow for a given pressure ratio. This leads to a smaller negative torque applied to the rotor and minor deceleration rate according to system of Equation 1 (brown curve in Figure 18). The computed time required to reduce speed at 60% is around 4.6s. The time spent in reverse flow using the cubic interpolation approximately the same of 1D method and is in the order of 3.75s. In this scenario the time spent on the left of the SLL would be 3.75s and thus according to the verification criteria additional protection device would be necessary.

Main outcome of present example is the importance of having a quite accurate description of the curve also on the left of the SLL for a safe and economic design ASV, protection devices and system piping. As a side consideration the simple criteria based on time spent on the left of SLL is probably not the best to account damaging related to surge cycles. More physical criteria is under investigation, based on number of surge cycles and vibrations associated to pressure waves during flow inversion.

ESD SIMULATION OF CO2 TRAIN

In this section a complete train with two compressors is considered for the validation of curve extension method, thanks to the availability of trends of pressure and speed measured at site during an ESD event. The experimental data are compared with those coming from the dynamic simulation. The system scheme is reported in Figure 19. The compressor train is composed by Steam Turbine, a double phase compressor equipped with 6 impellers (2MCL), a gear box and a second high pressure double phase compressor (2BCL), also equipped with six impeller. Due to the complexity of system layout, dynamic simulations are performed using a commercial tool and all the plant equipment (valve, coolers, ..) located between suction and discharge headers are included in the modelled environment.
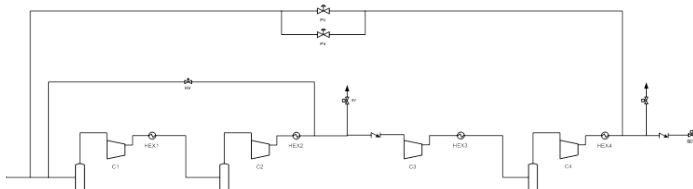

Figure 19 – System layout model

A method based on cubic model is used to provide extended compressor curves for the four phases of the compression train up to negative flow. The negative flow branch of the compressor curve is approximated with a valve-like parabolic characteristic having a non-zero head at zero flow and a second

order coefficient computed to provide the maximum pressure ratio with a mass flow equal to half the value corresponding to the maximum pressure. This trend can be easily inferred from Figure 5, considering shape of extended curve in the second quadrant. The computed trajectory of the operating point on head-flow compressor maps is shown in Figure 20 and indicates reverse flow transient in all the compressor stages. The first three stages stay for the majority of the ESD event in the reverse flow condition as a consequence of the characteristics of anti-surge loops but mainly the large volumes of the plant. Only the third phase experiences a surge cycle after reaching the limit stable point at zero reverse flow.
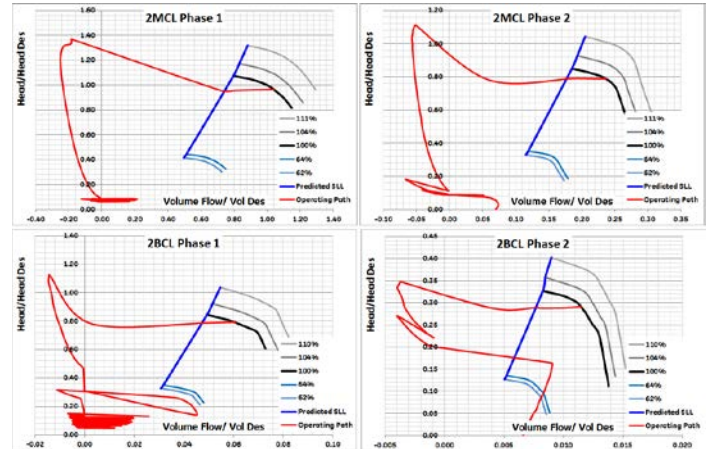

Figure 20 –Operating point transient trajectory during ESD

The measures at site during ESD are shown Figure 21 in terms of suction and discharge pressure trends (blue and green continuous lines respectively plotted on first axis) and speed values (red continuous curves plotted on secondary axis) for all compression stages. All pressures are made non dimensional with the inlet pressure of the compressor train and the speed with initial speed of first phase. The experimental trends of pressure do not show rapid pressure transients confirming that the three phases do not experience surge cycles. The only exception is the first phase of the 2BCL which seems to undergo a surge cycle after around 5s from trip. The measured speed after the acquisition time (30 seconds) is in the order of 10% of reference value.
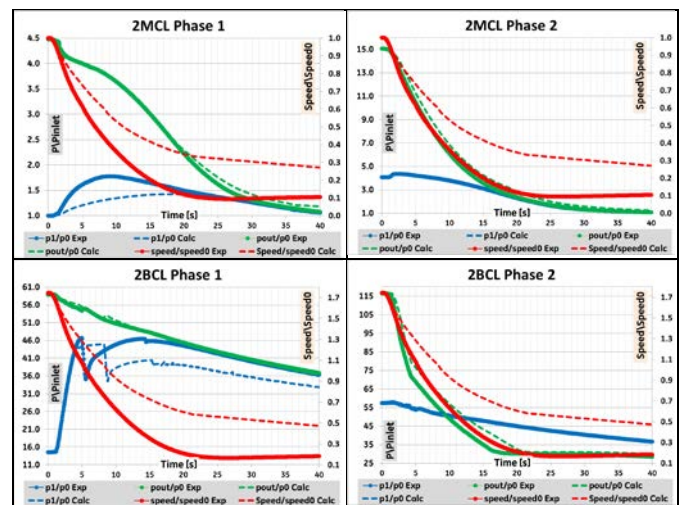

Figure 21 - Pressure and speed trend during site ESD event

In Figure 21 dotted lines represent the results obtained using the method based on cubic model. From the results of the calculations it can be seen that speed deceleration rate is smaller than the real one. After 30s the computations seem to indicate a final value of 20% for both rotors which is almost double with respect to the experimental ones.

To get a better agreement with site data the extension in the second quadrant the quadratic coefficient of the parabolic law has been modified to increase the gas torque in reverse flow. The mass flow which in the second quadrant corresponds to the maximum pressure is set to 85% of the value in direct flow. This value is consistent with Figure 10 reporting the comparison between 1D and cubic model for curve extension of model test in off design conditions. Final computations are reported in Figure 22 and show the improved agreement in speed trends and time derivatives. Time evolution of pressure is marginally affected by rotor speed for this compression train in view of large volumes as already observed for the previous test cases.
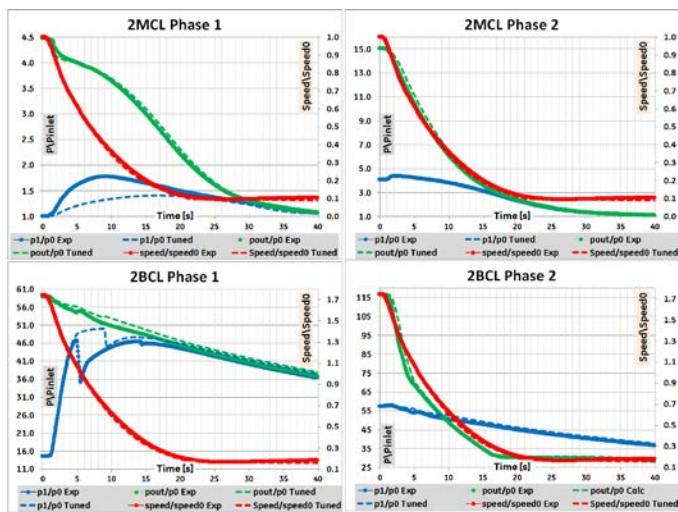

Figure 22 - Pressure and speed trends using tuned cubic law

This application indicates that 1D extension method used in the dynamic simulation could reproduce the observed site trends for rotational speed more accurately with respect to the classical cubic law based on a mathematical fitting. In particular the computation of absorbed power in reverse flow is confirmed to be quite underestimated using the cubic fitting as already observed for surge data from model test experiments.

CONCLUSIONS

Protection of systems equipped with centrifugal compressors from damages caused by surge is generally performed with a proper design of ASV which is usually a compromise between safety requirements and cost/complexity of the circuit layout. According to the authors experience compressor can be allowed operating on the left of the SLL for a limited time without damaging the main components. This includes the possibility of undergoing few surge cycles or operating in the stable reverse flow region provided that safety criteria are fulfilled. In this regard the description of the compressor characteristics in both the unstable positive slope region as also with negative flow may be required with a certain level of accuracy. Otherwise surge frequency, pressure fluctuations and speed trend during

ESD may be not so accurate to drive the proper design of the system. In this paper a simple method based on considerations about impeller velocity triangles has been investigated: despite the rough assumptions behind the scheme some basic features of system dynamics could be properly captured, in particular the impact of off design Mach conditions on the shape of reverse performance curve. Some analyzed system with large discharge volumes indicated that a stable reverse flow is experienced by the compressor during most of the time during ESD. This condition appears less critical for the compressor with respect to continuous cycling and may suggest that a design criteria based on time spent on the left of SLL is conservative. A verification criteria based on number of cycles could allow reducing complexity of surge protection devices and cost, still preserving safe operation of the system.

As far as concerns the system modeling the Greitzer scheme proved good accuracy in the description of basic harmonic content of surge phenomenon for some model test applications and allowed the verification and basic sizing of a relatively simple system. Higher frequency content related for instance to the propagation of acoustic pressure fluctuations and their impact on piping layout is not included. More complicated systems can be modelled using dynamic system modelling tools in which anyway the description of compressor curve is fundamental for the proper capturing of dynamic behavior.

NOMENCLATURE

D_1, D_2	Impeller Inlet/Outlet Diameter	[m]
V_1, V_2	Inlet and Outlet Volumes	[m3]
T_1, T_2	Inlet and Outlet Total Temperatures	[K]
P_1, P_2	Inlet and Outlet Pressures	[Pa]
c_2	Outlet Sound Speed	[m/s]
N	Rotational Speed	[RPM]
U_2	Impeller Tip Speed	[m/s]
$\overline{C_{P12}}$	Average Specific Heat	[kJ/kg]
ρ_{01}	Inlet Total Density	[kg/m³]
A_c	Compressor Inlet Area	[m²]
L_c	Compressor Reference Length	[m]
B	Stability Factor	
Z_1, Z_2	Inlet and Outlet Compressibility	
u_r	Valve Opening Ratio	
Greek letters		
ω_H	Helmotz Frequency	[Hz]
$\psi_{1,2}$	Inlet Outlet Pressure Coefficient	
$\psi_{C,V}$	Compressor/Valve Pressure Coefficient	
$\varphi_{C,V}$	Compressor/Valve Flow Coefficient	
ξ	Non dimensional Time	
γ	Isentropic exponent	

REFERENCES

[1] E. M. Greitzer, 1976 "Surge and Rotating Stall in Axial Flow Compressors- Part I and II.",@ J. Eng. Gas Turbines

Power 98(2), 190-198 (Apr 01, 1976).

[2] D. A. Fink, N. A. Cumpsty, E. M. Greitzer "Surge Dynamics in a Free-Spool Centrifugal Compressor System" @ Journal of Turbo machinery APRIL 1992, Vol. 11

[3] E. Belardini, D. T. Rubino, L. Tapinassi, A. Deponti, "Evaluation of Surge Pressure Dynamics in a Closed Fluid Circuit for Centrifugal Compressor Applications" @ International CAE Conference 2013

[4] K. Brun, R Kurz, M.G. Nored "Impact of Piping Impedance and Acoustic Characteristics on Centrifugal Compressor Surge and Operating Range "@ ASME Turbo Expo 2014, Düsseldorf

[5] K. Bammert, P. Zehner "Measurements of the Performance of an Air Turbine Stage at Positive and Negative Mass Flow and Rotational Speed (Four-Quadrant Characteristics)"@ Journal of Engineering for Power January 1978, VOL 100

[6] Moore, F. K., and Greitzer, E. M., 1986, "A Theory of Post-Stall Transients in Axial Compression Systems: Part I-Development of Equations," ASME J. Eng. Gas Turbines Power, 1986

[7] I. J. Day, E. M. Greitzer, N. A. Cumpsty,"Prediction of Compressor Performance in Rotating Stall", Journal of Engineering for Power JANUARY 1978

[8] Moore," A Theory of Rotating Stall of Multistage Axial Compressors: Part I - Small Disturbances", Journal of Engineering for Gas Turbines and Power APRIL 1984

[9] Moore," A Theory of Rotating Stall of Multistage Axial Compressors: Part II - Finite Disturbances", Journal of Engineering for Gas Turbines and Power APRIL 1984

[10] K. Bammed, P. Zehner," Measurements of the Performance of an Air Turbine Stage at Positive and Negative Mass Flow and Rotational Speed (Four-Quadrant Characteristics)", Journal of Engineering for Power JANUARY 1978

[11] M. Vahdati, G. Simpson and M. Imregun, M. "Unsteady flow and Aero-elasticity Behavior of Aero-Engine Core Compressors During Rotating stall and Surge", ASME paper GT2006-90308

[12] J. P. Longley, "Calculating Stall and Surge Transients", Proceedings of GT2007 ASME Turbo Expo 2007: Power for Land, Sea and Air

[13] K. K. Botros, D. Bakker, "Application of Three Methods in Determining the Effectiveness of Surge Protection Systems in Gas Compressor Stations", 2012 9th International Pipeline Conference

[14] N. G. Díez, J.P.M. Smeulers, L. Tapinassi, A, Scotti del Greco,L. Toni, "Predictability f rotating stall and surge in a centrifugal compressor stage with dynamic simulations", 2014 ASME Turbo Expo

[15] Koff, S. G., and Greitzer, E. M., "Axisymmetrically Stalled Flow Performance for Multistage Axial Compressors," ASME Journal of Turbomachinery, Vol. 108, 1986, pp. 216-223